Talanta 179 (2018) 531–537

Contents lists available at ScienceDirect

Talanta

journal homepage: www.elsevier.com/locate/talanta

A novel peptide/Fe_3O_4@SiO_2-Au nanocomposite-based fluorescence biosensor for the highly selective and sensitive detection of prostate-specific antigen

Lanfang Yang, Nan Li, Ke Wang, Xiaoman Hai, Junxia Liu, Fuquan Dang*

Key Laboratory of Analytical Chemistry for Life Science of Shaanxi Province, School of Chemistry and Chemical Engineering, Shaanxi Normal University, 620 West Chang'an Street, Xi'an 710119, China

ARTICLE INFO

Keywords:
PSA
Fe_3O_4@SiO_2-Au nanocomposites
5-FAM labeled peptides
Fluorescence

ABSTRACT

Highly selective and sensitive detection methods are very important for the early diagnosis of prostate-specific antigen (PSA). Here, we present a novel peptide/Fe_3O_4@SiO_2-Au nanocomposite-based fluorescence biosensor for highly selective and sensitive detection of PSA. The biosensor was made by self-organizing 5-FAM labeled peptides onto the surface of magnetic Fe_3O_4@SiO_2-Au nanocomposites (MNCPs), resulting in efficient quenching of the FAM fluorescence. The PSA specifically recognized and cleaved the 5-FAM-labeled peptides, leading to the fluorescence recovery. This is the first report of the MNCPs by in situ growth of Au nanoparticles (AuNPs) on the SiO_2 encapsulated single Fe_3O_4 nanocubes. The MNCPs feature robust salt stability, and allow for effective fluorescence quenching and easy magnetic separation, which greatly decrease the background fluorescence. The peptide/MNCPs-based fluorescence biosensor measure a wide range of concentrations of PSA, from 1.0×10^{-12} to 1.0×10^{-9} g/mL, with a limit of detection (LOD) of 3.0×10^{-13} g/mL in both standard solutions and serum samples, demonstrating the great potential of this biosensor platform for use in clinical and biological assays.

1. Introduction

Prostate cancer is a fairly common malignancy with mortality rates ranked second out of various cancers in men [1–6]. Early and precise diagnosis of tumor biomarkers will be of great help for the cancer therapy [7–10]. However, the levels of tumor biomarkers are often remarkably low in biological samples obtained from patients during early disease progression [11,12]. Currently, prostate-specific antigen (PSA) is widely used in the early diagnosis of prostate cancer [13–15]. There is the great possibility for people with more than 4 ng/mL of PSA in serum suffering from prostate cancer [16–18]. Therefore, it is imperative to explore a highly selective and sensitive determination method for detection and quantification of PSA. The conventional immunoassay methods, such as surface plasmon resonance [19], electrogenerated chemiluminescence (ECL) [20,21], electrochemical immunoassay [22], and fluorescence [23] are developed for monitoring serum PSA. Among these techniques, fluorescence immunoassay has attracted much attention due to its merits, including facile process and high sensitivity [24]. However, the existing fluorescence immunoassays are largely based on antibodies as recognition elements, which generally involve several weaknesses including high cost, high time consumption, and easy denaturalization and deactivation [25].

Recently, oligopeptides with specific sequences have emerged as a compelling alternative to antibodies for protein assays. Oligopeptides have many advantages over antibodies, such as cost-effectiveness, stability, reliability, resistance to harsh environments, and facile chemical synthesis [26,27]. Since PSA has shown molecular recognition and enzymatic activity for an oligopeptide (HSSKLQ) [28], several peptide-based methods have been proposed for the PSA detection with high specificity, including ECL, electrochemical, and fluorescence assays [29–31]. Among these approaches, peptide-based fluorescence methods have aroused some interest due to its rapidity, simplicity, and wide linear range. For instance, Choi et al. constructed a peptide-based fluorescence biosensor using gold nanoparticles (AuNPs) as the quencher for measuring the enzyme activity of PSA, in which AuNPs must be centrifuged to facilitate detection. Generally, AuNPs are laborious to separate and possess poor salt stability [32,33], tending to readily agglomerate and impair the performance of AuNPs-based biosensors. Thus, the development of functional AuNPs-based nanocomposites is necessary to achieve highly selective and sensitive detection of PSA.

To date, various materials including metal-organic frameworks

* Corresponding author.
E-mail address: dangfqn@snnu.edu.cn (F. Dang).

https://doi.org/10.1016/j.talanta.2017.11.033
Received 21 September 2017; Received in revised form 27 October 2017; Accepted 17 November 2017
Available online 21 November 2017
0039-9140/

(MOFs) [34,35], silicon nanowires (SiNWs) [36], PbS [37], Ag [38], Pd [39], SiO_2 [40,41], and Fe_3O_4 [42,43] have been explored in the construction of functional AuNPs-based nanocomposites. Among these, SiO_2 is a promising material to improve the salt stability of AuNPs, due to its good hydrophilicity, biocompatibility, and mature surface functionalization [44–46]. Fe_3O_4 can be used simultaneously to simply and rapidly separate interfering molecules [47–49]. Therefore, magnetic Fe_3O_4@SiO_2-Au nanocomposites (MNCPs) might be an ideal platform for monitoring the enzyme activity of PSA with high specificity. The main objective of this work is to develop a peptide/MNCPs-based fluorescence biosensor for the highly selective and sensitive detection of PSA. A specific oligopeptide (CHSSKLQK) labeled by 5-FAM (FAM-peptides) was designed as a fluorescence emitting and molecular recognition element, and MNCPs were used as the fluorescence quenchers and magnetic splitters. The MNCPs significantly exhibit excellent stability at high salt concentrations (0.1 M), and allow for the effective quenching to FAM-peptides and facile magnetic separation from solution, which greatly decrease the background fluorescence. In the presence of PSA, the FAM-peptides are specifically recognized and cleaved by PSA, releasing the fluorescence emitting species from the MNCPs surface and leading to the recovery of fluorescence. Thus, highly selective and sensitive detection of PSA, both in standard solutions and serum samples, was achieved using this peptide/MNCPs-based fluorescence biosensor.

2. Experimental section

2.1. Chemicals

FAM-peptides were synthesized by Shanghai Apeptide Co., Ltd. (China). Myoglobin (Mb) were obtained from Abcam Inc. (Cambridge, United Kingdom). PSA from human semen, thrombin (Thb), lysozyme (LYZ), glucose oxidase (GOD) , β-lactoglobulin (β-LAG), bovine serum albumin (BSA), chloroauric acid ($HAuCl_4$), polyoxyethylene (5) nonylphenylether (IgepalCO-520), 3-aminopropyltriethoxysilane (APTES), and sodium borohydride ($NaBH_4$, 99%) were all purchased from Sigma-Aldrich. Iron chloride ($FeCl_3{\cdot}6H_20$, 99%) , sodium oleate ($C_{17}H_{33}CO_2Na$, 96%), 1-octadecene ($C_{18}H_{36}$, 90%), aqueous ammonia (25–28%), and tetraethyl orthosilicate (TEOS, 98%) were purchased from Sinopharm Chemical Reagent Ltd. A solution of 10 mM phosphate-buffered saline (PBS) was made up using 10 mM Na_2HPO_4, 10 mM NaH_2PO_4, and 10 mM NaCl (pH 7.4). A Millipore filtration system was used to provide the DI water in the experiments.

2.2. Instrumentation

Transmission electron micrograph (TEM) experiments were performed on a JEM-2100 transmission electron microscope (JEOL, Japan). A Kratos Analytical Axis Ultra photoelectron spectrometer (Kratos Analytical ltd, UK) was used for the X-ray photoelectron spectroscopy (XPS) measurements. Energy-dispersive X-ray analysis (EDX) was conducted with an environmental scanning electron microscopy (FEI Quanta 200). The fluorescence spectra were obtained from 500 to 600 nm with an excitation at 486 nm using a LS 55 Fluorescence Spectrometer. All fluorescence spectra were measured at least in triplicate.

2.3. Synthesis of hydrophobic Fe_3O_4 nanocubes

The $C_{54}H_{99}FeO_6$ was first synthesized according to the method reported by Park et al. [50]. Briefly, $C_{18}H_{33}NaO_2$ (36.5 g) and $FeCl_3{\cdot}6H_2O$ (10.8 g) were added into a mixture of hexane (140 mL), DI water (60 mL), and ethanol (80 mL). The mixture was reacted to 60 °C and refluxed for 4 h. After cooling to 25 °C, the resulting waxy $C_{54}H_{99}FeO_6$ was washed with DI water. To synthesize Fe_3O_4 nanocubes [51], the $C_{18}H_{33}NaO_2$ (0.64 g) and $C_{54}H_{99}FeO_6$ (1.8 g) were added to a three-necked flask (50 mL) with a solvent of 1-octadecene (10 g). The mixture was kept at 200 °C for 1 h and then at 320 °C for 40 min. The reaction solution needs to be rapidly cooled to 25 °C, and the resulting Fe_3O_4 nanocubes were washed with hexane and ethanol. Afterward, the product was vacuum-dried at 60 °C for 12 h.

2.4. Synthesis of NH_2-modified Fe_3O_4@SiO_2 nanoparticles

A reversal microemulsion technique was used to synthesize the Fe_3O_4@SiO_2 nanoparticles [52]. Fe_3O_4 (0.0019 g) and Igepal-CO 520 (0.52 g) were mixed in cyclohexane (11 mL). Afterward, $NH_3{\cdot}H_2O$ (0.2 mL, 28–30%) and TEOS (0.28 mL) were added to the solution with continuous stirring. The resulting Fe_3O_4@SiO_2 nanoparticles were centrifuged, washed with ethanol and hexane, and finally redispersed in ethanol. Finally, APTES was dropped into an ethanol solution of Fe_3O_4@SiO_2 nanoparticles to react for 24 h. The NH_2-modified Fe_3O_4@SiO_2 nanoparticles were centrifuged, and washed with ethanol and DI water.

2.5. Preparation of MNCPs

These MNCPs were synthesized on the basis of a reported procedure [53]. The NH_2-modified Fe_3O_4@SiO_2 nanoparticles (0.008 g) were redispersed in DI water (20 mL), and mixed with 1 wt% $HAuCl_4$ aqueous solution (0.5 mL). After stirring at 25 °C for 1 h, 50 mM $NaBH_4$ solution (10 mL) was dropped into the reaction mixture, and kept the stirring for another 1 h. The products were centrifuged, washed with copious DI water, and finally dried at 60 °C for 8 h.

2.6. PSA detection

Scheme 1 illustrates the schematic of peptide/MNCPs-based fluorescence biosensor for the PSA detection. FAM-peptides were self-organized on the surface of MNCPs via Au-S bonds, leading to the efficient quenching of FAM fluorescence by the AuNPs. In the presence of the target, PSA specifically cleaved the FAM-peptides and released the fluorescence emitting species from the MNCPs surface, which led to the fluorescence recovery.

2.6.1. Fluorescence quenching by MNCPs

In fluorescence quenching experiments, different volumes of MNCPs (200 μg/mL) were mixed with 20 μL of FAM-peptides (10 μM) in 10 mM PBS and the volumes were adjusted to 200 μL with 10 mM PBS for further fluorescence detection. The mixture was kept with oscillation at 25 °C for 0.5 h before testing. The final concentrations of MNCPs in the cuvettes were 0, 10, 20, 30, 40, 50, 60, 80, 100, and 150 μg/mL.

2.6.2. Fluorescence recovery by PSA

In fluorescence-recovery experiments, a variable amount of PSA (1.0×10^{-9} g/mL) and 20 μL of FAM-peptides (10 μM) in 10 mM PBS were thoroughly mixed and kept at 37 °C for 1 h. An aliquot of 30 μL MNCPs (200 μg/mL) in 10 mM PBS was introduced and the volumes were adjusted to 200 μL with 10 mM PBS. Finally, the mixture was kept at 25 °C with oscillation for 0.5 h before testing.

3. Results

3.1. Characterization of materials

TEM, XPS, and EDX were first performed to determine the features of the materials and confirm the synthesis of MNCPs. Monodisperse Fe_3O_4 nanocubes of ca. 12 nm were successfully synthesized by thermal decomposition of the iron-oleate [51] (Fig. 1A). As shown in Fig. 1B, the uniform sphere-shaped Fe_3O_4@SiO_2 nanoparticles of ca. 38 nm were readily prepared by encapsulating single Fe_3O_4 nanocubes with the SiO_2 shells of ca. 13 nm using a reversal microemulsion technique

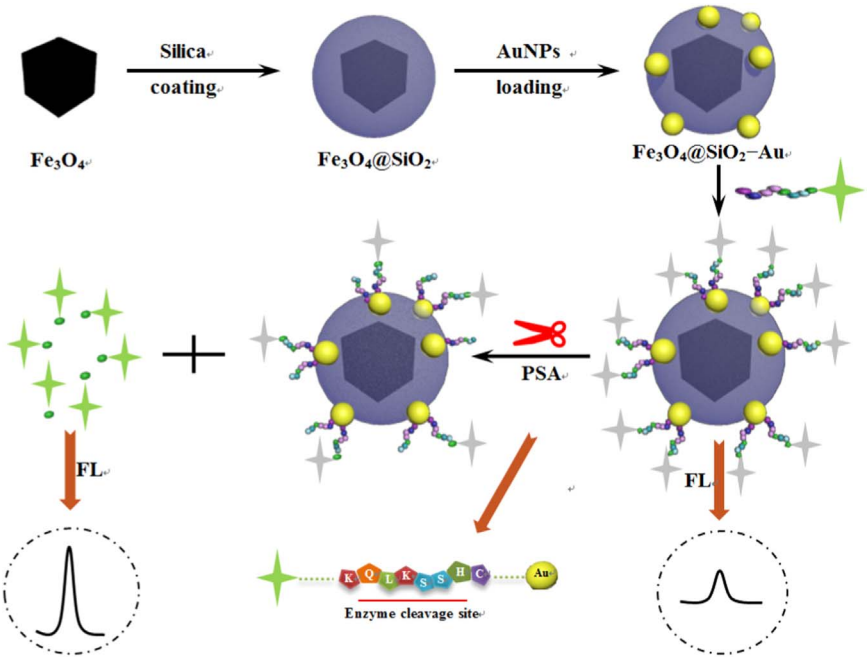

Scheme 1. Schematic diagram of a peptide/MNCPs-based fluorescence biosensor for the determination of PSA.

[52]. The hydrophilicity and biocompatibility of SiO_2 shells can efficiently avoid particles agglomeration, facilitating future functionalization and applications. Then, AuNPs of 6–12 nm were grafted onto the NH_2-modified $Fe_3O_4@SiO_2$ nanoparticles through a sodium borohydride reduction method [53], forming well-defined MNCPs of ca. 56 nm (Fig. 1C), which can be easily separated from a water suspension under the magnetic field (Fig. 1D). The remaining supernatant is transparent, confirming that the MNCPs are magnetic and can be used as a magnetic splitter. Compared to the previously reported biosensors, the peptide/MNCPs-based fluorescence biosensor allows for facile magnetic separation form the solution , which can greatly decrease the fluorescence interference. The XPS spectrum of MNCPs is shown in Fig. 1E. The existence of AuNPs was indicated by the Au 4f peak at 81.0 eV, while the characteristic Si 2p peak at 100.0 eV and the Fe 2p peak at 710.0 eV verified the presence of the SiO_2 shell and the core Fe_3O_4, respectively, confirming the successful fabrication of MNCPs. EDX measurements revealed that the MNCPs are composed of C (16.15%), N (5.81%), O (44.69%), Si (20.81%), Fe (5.21%), and Au (7.33%), providing further evidence for the TEM and XPS observations of the successful construction of MNCPs (Fig. 1F).

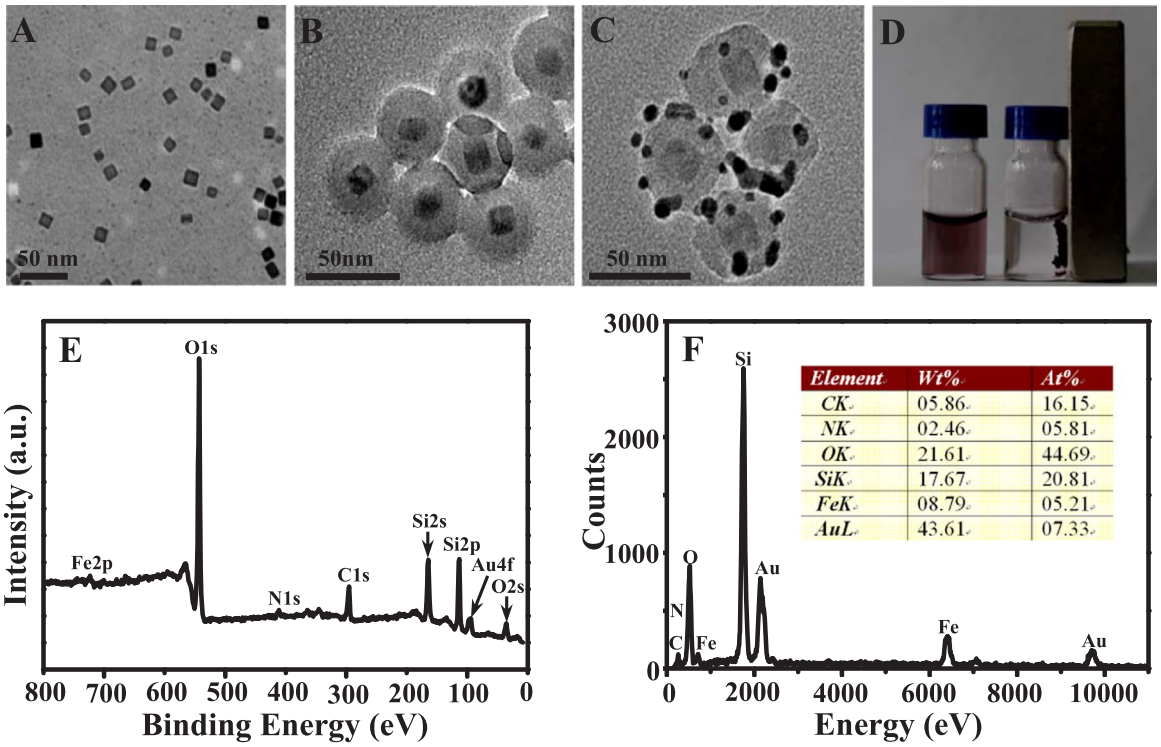

Fig. 1. TEM images of: (A) Fe_3O_4 nanocubes; (B) $Fe_3O_4@SiO_2$ nanoparticles; (C) MNCPs. (D) Photographic image of MNCPs in DI water before and after magnetic separation. (E) XPS spectrum of MNCPs. (F) EDX pattern of the MNCPs.

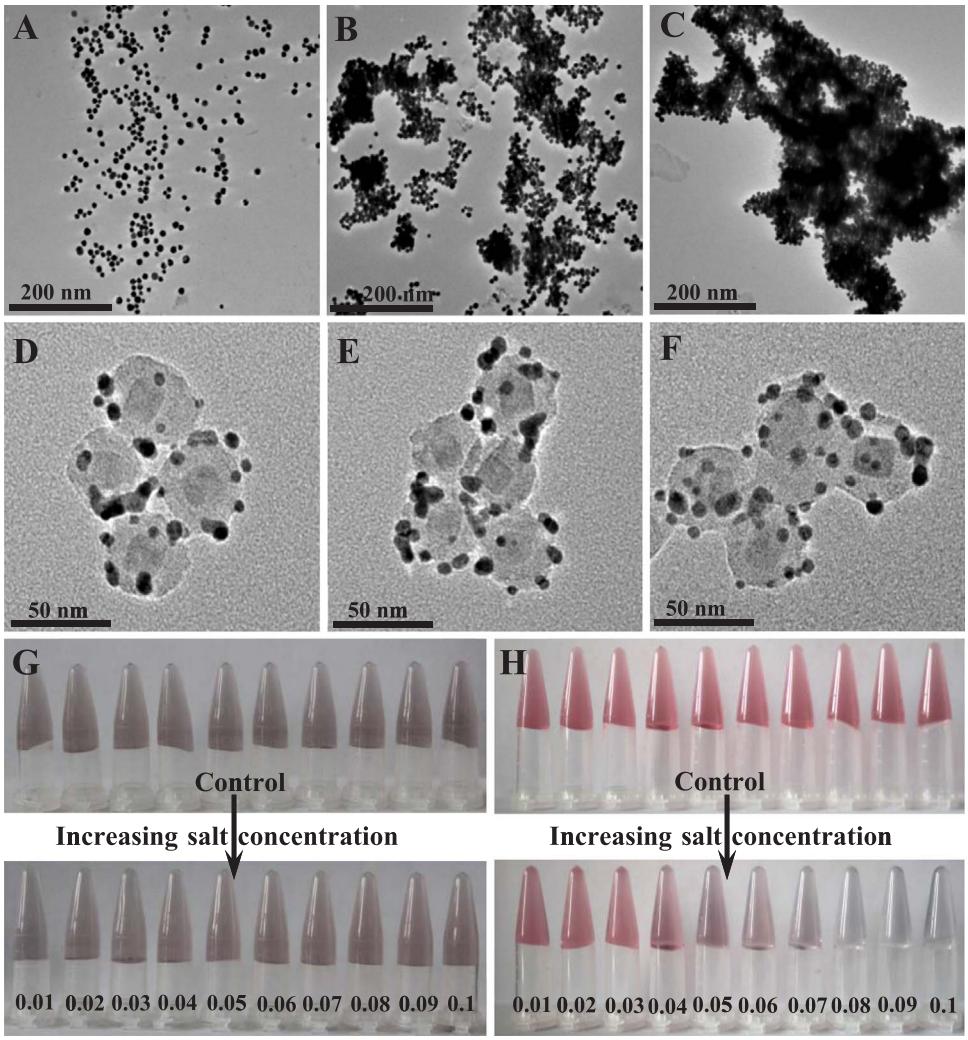

Fig. 2. TEM images of free AuNPs (A-C) and MNCPs (D-F) in NaCl solutions of 0, 0.04, and 0.08 M (left to right). (G, H) Photographs of the MNCPs or AuNPs solutions with various concentrations of NaCl (0.01–0.1 M).

3.2. Verification of salt stability

Generally, AuNPs-based biosensors possess poor salt stability, since AuNPs readily agglomerate in salt concentrations over 0.01 M, which greatly decreases the biosensor's performance and limits their wide applications. Although the aqueous solution of free AuNPs is fairly steady (Fig. 2A), AuNPs steadily agglomerated as the salt concentration increases (Fig. 2B, C), since concentrated salt can greatly decrease electrostatic repellency between AuNPs [54]. Contrarily, the MNCPs exhibit very good salt stability, and no obvious agglomeration of AuNPs was observed even in a high salt solution of 0.08 M (Fig. 2D-F). The color of MNCPs solutions kept red-brown (Fig. 2G) whereas the color of AuNPs solutions gradually shifted from red to blue in 0.01–0.1 M salt solutions (Fig. 2H), verifying excellent stability and dispersibility of MNCPs over AuNPs against salt induced aggregation [36]. Obviously, the strong salt stability of MNCPs is largely attributed to the hydrophilic SiO_2 shells, which efficiently avoid the agglomeration of AuNPs. The excellent stability and dispersibility of MNCPs over AuNPs is crucial for the PSA detection in real bio-samples generally with high-concentration salt.

3.3. Feasibility study

The fluorescence spectra measurements under different conditions were first performed to validate the feasibility of the peptide/MNCPs-based biosensor. As shown in Fig. 3A, the FAM-peptides (1 μM) showed a strong fluorescence emission at 522 nm (line a), which is used as a control. When PSA of 5.0×10^{-11} g/mL was added, no obvious change in fluorescence intensity was observed as compared to that of the control (line b), suggesting the negligible effect of PSA on the FAM fluorescence. The fluorescence intensity of FAM-peptides was greatly decreased with the addition of MNCPs (line d), which was about 20% of FAM-peptides alone. This result indicates that MNCPs can efficiently quench the fluorescence of FAM-peptides. When MNCPs were introduced to a solution of 1 μM FAM-peptides and 5.0×10^{-11} g/mL PSA, the fluorescence of 81.7% was kept as compared with that of the control (line c), indicating that PSA can efficiently recognize and cleave the FAM-peptides attached on MNCPs. These results show that MNCPs can be used as an ideal sensing platform for PSA. The selectivity of the peptide/MNCPs-based fluorescence biosensor using MNCPs (30 μg/mL) was evaluated by measuring PSA (5.0×10^{-10} g/mL) and interfering proteins (5.0×10^{-9} g/mL), including myoglobin (Mb), thrombin (THF), lysozyme (LYZ), glucose oxidase (GOD), β-lactoglobulin (β-LAG), and bovine serum albumin (BSA), respectively. Compared with the fluorescence intensity of FAM-peptides (1 μM) under the same experimental conditions, fluorescence intensity changes greatly for PSA (5.0×10^{-10} g/mL) but interfering proteins (5.0×10^{-10} g/mL), suggesting that the tested interfering proteins did not significantly affect the PSA detection (Fig. 3B).

3.4. Fluorescence detection of PSA

3.4.1. Fluorescence quenching of FAM-peptides by MNCPs

Fig. 4A shows the fluorescence spectra of 1 μM FAM-peptides in the

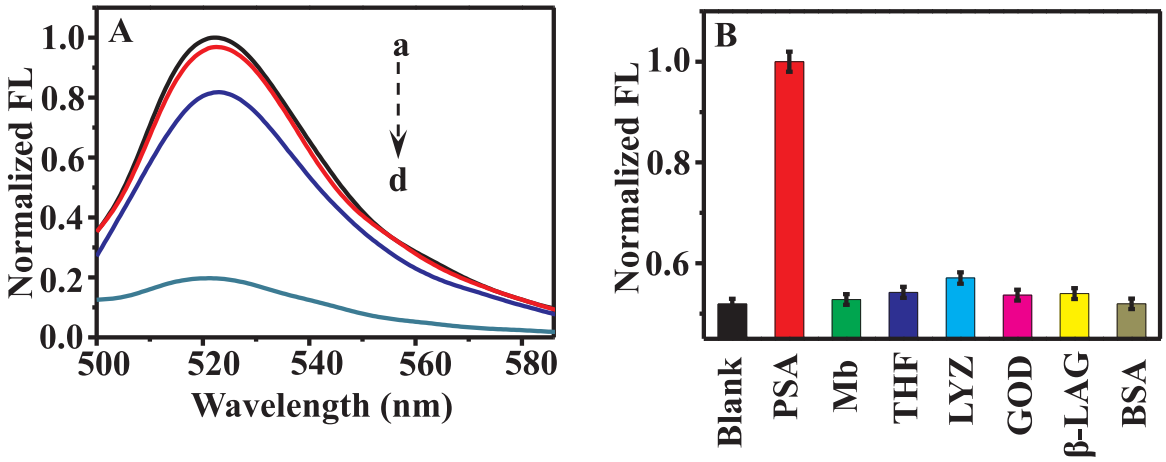

Fig. 3. (A) Fluorescence emission spectra of FAM-peptides (1 μM) under different conditions: (a) FAM-peptides in 10 mM PBS; (b) FAM-peptides and 5 × 10^{-11} g/mL PSA; (c) FAM-peptides, 5 × 10^{-11} g/mL PSA and MNCPs; (d) FAM-peptides and MNCPs. (B) Fluorescence intensity of the FAM-peptides (1 μM) and MNCPs (30 μg/mL) in the presence of (5.0 × 10^{-10} g/mL) PSA (5.0 × 10^{-10} g/mL) and interfering proteins (5.0 × 10^{-9} g/mL) including Mb, THF, LYZ, GOD, β-LAG, and BSA, respectively.

presence of 0−150 μg/mL MNCPs in 10 mM PBS. The fluorescence intensity of FAM-peptides at 522 nm decreased gradually with increasing MNCPs, suggesting that FAM-peptides were readily self-organized onto the surface of MNCPs. The fluorescence of ~80% was quenched by 100 μg/mL MNCPs, and no significant increase in fluorescence quenching was obtained with MNCPs higher than 100 μg/mL (Fig. 4B). The effective fluorescence quenching and facile magnetic separation by MNCPs greatly minimize the fluorescence background and thus allow for the sensitive PSA detection.

3.4.2. FAM-peptides/PSA interaction analysis

Fluorescence recovery experiments were performed to investigate the interaction of FAM-peptides with PSA. MNCPs of 30 μg/mL corresponding to ~50.5% fluorescence quenching were used to carry out the recovery experiments. MNCPs were mixed with the solution of FAM-peptides and PSA to study their effect on fluorescence. With the final concentration of the FAM-peptides and MNCPs fixed at 1 μM and 30 μg/mL respectively, the fluorescence intensity of the FAM-peptides increased with increasing PSA concentration over a range of 1 × 10^{-12} − 1 × 10^{-9} g/mL (Fig. 5A). The fluorescence intensity eventually reached ~ 94% of that of the control with 1.0 × 10^{-9} g/mL PSA. An excellent linear relationship was obtained between the normalized fluorescence intensity and the logarithm of the PSA concentration over 1.0 × 10^{-12} to 1.0 × 10^{-9} g/mL (Fig. 5B). The linear equation follows $Y = 0.29746X + 3.66447$ ($R^2 = 0.99509$), where Y is the normalized fluorescence intensity and X is the logarithm of the PSA concentration. The detection limit (LOD) is 3.0 × 10^{-13} g/mL (defined as 3 × the standard deviation of the blank) and the quantitation limit is 9.9 × 10^{-13} g/mL (defined as 10 × the standard deviation of the blank), which is lower than conventional fluorescence probes (a list of additional methods is provided in Table S1). These results strongly suggest that MNCPs are an ideal sensing platform for monitoring PSA.

3.5. Analysis of real samples

The feasibility of the peptide/MNCPs-based fluorescence biosensor for analysis of real samples was evaluated using serum samples from healthy volunteers. The clinical serum samples, which were provided by a local hospital according to the provisions of the local ethics committee, were diluted 100-fold with 10 mM PBS. First, various doses of PSA (1.0 × 10^{-9} g/mL) and 20 μL of FAM-peptides (10 μM) were mixed with serum samples completely. Next, 30 μL of MNCPs (200 μg/mL) was added into the mixture. The final concentrations of PSA in serum samples were 2.5 × 10^{-11}, 5.0 × 10^{-11}, and 1.0 × 10^{-10} g/mL while those of the FAM-peptides and MNCPs were respectively kept at 1 μM and 30 μg/mL. The recoveries of PSA in serum samples were 98.4%, 102.8%, and 101.9%, respectively (Table S2). The reproducibility and precision of the peptide/MNCPs-based fluorescence biosensor were evaluated by assaying 2.5 × 10^{-11}, 5.0 × 10^{-11}, and 1.0 × 10^{-10} g/mL PSA in serum examples. Experimental results indicated that the coefficients of variation (CVs) of the intra-assay and inter-assay were below 4.7% ($n=6$) and 8.2% ($n=6$), respectively (Table S3),

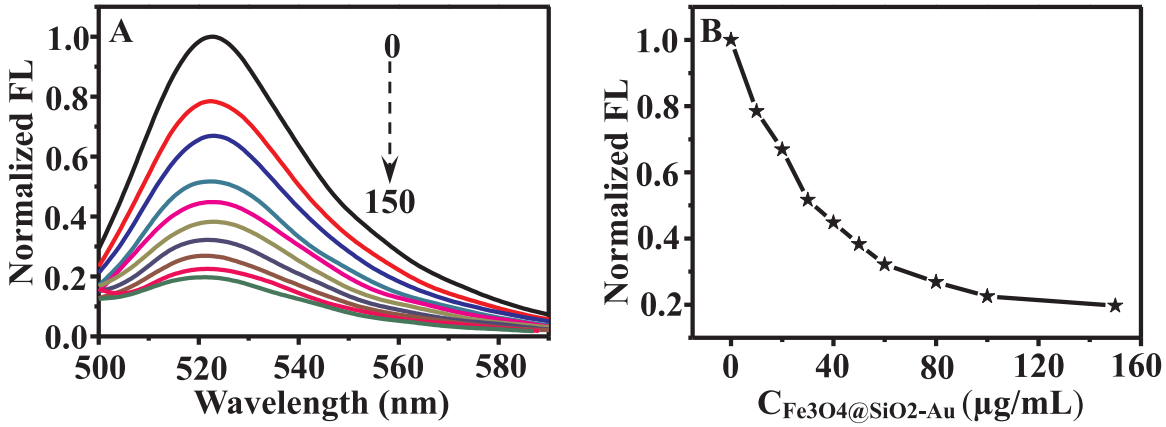

Fig. 4. (A) Fluorescence intensity of the FAM-peptides (1 μM) upon the introduction of different concentrations of MNCPs (0, 10, 20, 30, 40, 50, 60, 80, 100, and 150 μg/mL) in PBS. (B) Fluorescence intensity of FAM-peptides versus concentration of MNCPs.

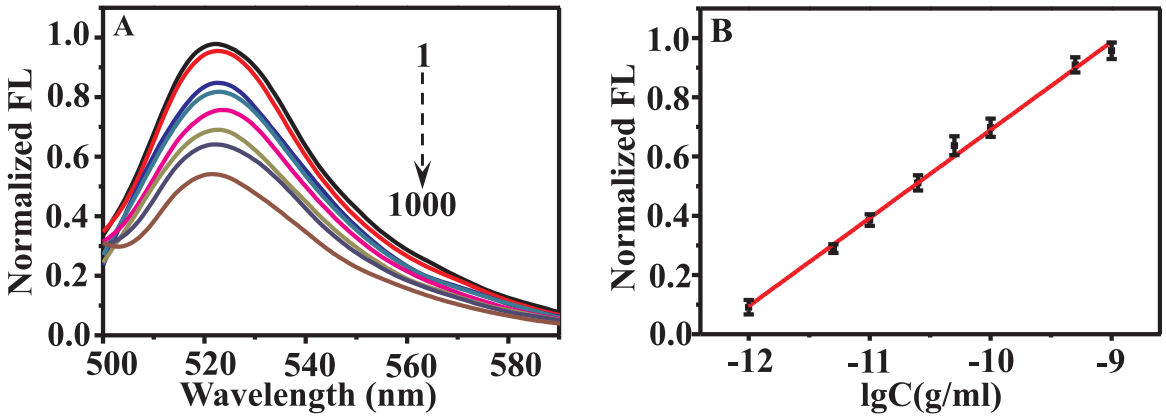

Fig. 5. (A) Fluorescence spectra of FAM-peptides (1 μM) and MNCPs (30 μg/mL) in the presence of different concentrations of PSA (1×10^{-12}, 5×10^{-12}, 1×10^{-11}, 2.5×10^{-11}, 5×10^{-11}, 1×10^{-10}, 5×10^{-10}, 1×10^{-9} g/mL). (B) The calibration curve between the normalized fluorescence intensity and the logarithm of the PSA concentration. The concentrations of PSA were 1×10^{-12}, 5×10^{-12}, 1×10^{-11}, 2.5×10^{-11}, 5×10^{-11}, 1×10^{-10}, 5×10^{-10}, 1×10^{-9} g/mL.

indicating its great potential for analysis of real samples.

4. Conclusion

In summary, we developed a novel peptide/MNCPs-based fluorescence biosensor for the PSA detection with high sensitivity and selectivity. FAM-peptide was designed as a fluorescence emitting and molecular recognition element, and MNCPs were used as the fluorescence quenchers and magnetic splitters. The MNCPs exhibit excellent salt stability and dispersibility, and allow for the efficient quenching of FAM-peptides and easy magnetic separation in solution, which greatly decrease the background fluorescence. The MNCPs-based fluorescence biosensor allows for highly selective measurement of PSA from 1.0×10^{-12} to 1.0×10^{-9} g/mL with a LOD of 3.0×10^{-13} g/mL in both standard solutions and serum samples , and the CVs of intra-assay and inter-assay are less than 4.7% ($n=6$) and 8.2% ($n=6$), respectively, indicating promising potential of the proposed fluorescence biosensor in clinical and biological assays. This work provides the framework for the development of highly selective and sensitive fluorescence biosensors by employing the direct transduction of peptide cleavage events and MNCPs as a sensing platform for other tumor markers with enzymatic cleavage activity.

Acknowledgments

This work was supported by the National Natural Science Foundation of China (No. 21175088).

Appendix A. Supporting information

Supplementary data associated with this article can be found in the online version at http://dx.doi.org/10.1016/j.talanta.2017.11.033.

References

[1] A. Jemal, R. Siegel, J.Q. Xu, E. Ward, Cancer statistics, 2010, CA Cancer J. Clin. 60 (2010) 277–300.
[2] M.M. Center, A. Jemal, J. Lortet-Tieulent, E. Ward, J. Ferlay, O. Brawley, F. Bray, International variation in prostate cancer incidence and mortality rates, Eur. Urol. 61 (2012) 1079–1092.
[3] J. Ferlay, E. Steliarova-Foucher, J. Lortet-Tieulent, S. Rosso, J. Coebergh, H. Comber, D. Forman, F. Bray, Cancer incidence and mortality patterns in Europe: estimates for 40 countries in 2012, Eur. J. Cancer 49 (2013) 1374–1403.
[4] A. Fuerea, G. Baciarello, A. Patrikidou, L. Albigès, C. Massard, M. Di Palma, B. Escudier, K. Fizazi, Y. Loriot, Early PSA response is an independent prognostic factor in patients with metastatic castration-resistant prostate cancer treated with next-generation androgen pathway inhibitors, Eur. J. Cancer 61 (2016) 44–51.
[5] E. Çevik, Ö. Bahar, M. Şenel, M.F. Abasıyanık, Construction of novel electrochemical immunosensor for detection of prostate specific antigen using ferrocene-PAMAM dendrimers, Biosens. Bioelectron. 86 (2016) 1074–1079.
[6] Y.C. Wei, X.J. Li, X. Sun, H.M. Ma, Y. Zhang, Q. Wei, Dual-responsive electrochemical immunosensor for prostate specific antigen detection based on Au-CoS/graphene and CeO_2/ionic liquids doped with carboxymethyl chitosan complex, Biosens. Bioelectron. 94 (2017) 141–147.
[7] S.M. Hanash, C.S. Baik, O. Kallioniemi, Emerging molecular biomarkers—blood-based strategies to detect and monitor cancer, Nat. Rev. Clin. Oncol. 8 (2011) 142–150.
[8] A. Guo, Y. Li, W. Cao, X. Meng, D. Wu, Q. Wei, B. Du, An electrochemical immunosensor for ultrasensitive detection of carbohydrate antigen 199 based on Au@Cu_xOS yolk–shell nanostructures with porous shells as labels, Biosens. Bioelectron. 63 (2015) 39–46.
[9] Z. Wang, N. Liu, F. Feng, Z. Ma, Synthesis of cadmium, lead and copper alginate nanobeads as immunosensing probes for the detection of AFP, CEA and PSA, Biosens. Bioelectron. 70 (2015) 98–105.
[10] J.H. Feng, Y.Y. Li, M.D. Li, F.Y. Li, J. Han, Y.H. Dong, Z.W. Chen, P. Wang, H. Liu, Q. Wei, A novel sandwich-type electrochemical immunosensor for PSA detection based on PtCu bimetallic hybrid (2D/2D) rGO/g-C_3N_4, Biosens. Bioelectron. 91 (2017) 441–448.
[11] S. Nagrath, L.V. Sequist, S. Maheswaran, D.W. Bell, D. Irimia, L. Ulkus, M.R. Smith, E.L. Kwak, S. Digumarthy, A. Muzikansky, Isolation of rare circulating tumour cells in cancer patients by microchip technology, Nature 450 (2007) 1235–1239.
[12] D.A. Giljohann, C.A. Mirkin, Review article drivers of biodiagnostic development, Nature 462 (2009) 461–464.
[13] A. Salimi, B. Kavosi, F. Fathi, R. Hallaj, Highly sensitive immunosensing of prostate-specific antigen based on ionic liquid–carbon nanotubes modified electrode: application as cancer biomarker for prostatebiopsies, Biosens. Bioelectron. 42 (2013) 439–446.
[14] F.Y. Li, Y.Y. Li, J.H. Feng, Y.H. Dong, P. Wang, L. Chen, Z.W. Chen, H. Liu, Q. Wei, Ultrasensitive amperometric immunosensor for PSA detection based on Cu_2O@CeO_2-Au nanocomposites as integrated triple signal amplification strategy, Biosens. Bioelectron. 87 (2017) 630–637.
[15] D.D. Xu, Y.L. Deng, C.Y. Li, Y. Lin, H.W. Tang, Metal-enhanced fluorescent dye-doped silica nanoparticles and magnetic separation: a sensitive platform for one-step fluorescence detection of prostate specific antigen, Biosens. Bioelectron. 87 (2017) 881–887.
[16] I. Strzeminska, S. Sainte Rose Fanchine, G. Anquetin, S. Reisberg, V. Noel, M.C. Pham, B. Piro, Grafting of a peptide probe for prostate-specific antigen detection using diazonium electroreduction and click chemistry, Biosens. Bioelectron. 81 (2016) 131–137.
[17] L.H. Pan, S.H. Kuo, T.Y. Lin, C.W. Lin, P.Y. Fang, H.W. Yang, An electrochemical biosensor to simultaneously detect VEGF and PSA for early prostate cancer diagnosis based on graphene oxide/ssDNA/PLLA nanoparticles, Biosens. Bioelectron. 89 (2017) 598–605.
[18] K. Yang, Y.J. Hu, N. Dong, G.C. Zhu, T.F. Zhu, N.J. Jiang, A novel SERS-based magnetic aptasensor for prostate specific antigen assay with high sensitivity, Biosens. Bioelectron. 94 (2017) 286–291.
[19] Y. Uludag, I.E. Tothill, Cancer biomarker detection in serum samples using surface plasmon resonance and quartz crystal microbalance sensors with nanoparticle signal amplification, Anal. Chem. 84 (2012) 5898–5904.
[20] N.P. Sardesai, J.C. Barron, J.F. Rusling, Carbon nanotube microwell array for sensitive electrochemiluminescent detection of cancer biomarker proteins, Anal. Chem. 83 (2011) 6698–6703.
[21] K. Shao, J. Wang, X.C. Jiang, F. Shao, T.T. Li, S.Y. Ye, L. Chen, H.Y. Han, Stretch–stowage–growth strategy to fabricate tunable triply-amplified electrochemiluminescence immunosensor for ultrasensitive detection of pseudorabies virus antibody, Anal. Chem. 86 (2014) 5749–5757.
[22] L. Han, C.M. Liu, S.L. Dong, C.X. Du, X.Y. Zhang, L.H. Li, Y. Wei, Enhanced conductivity of rGO/Ag NPs composites for electrochemical immunoassay of prostate-specific antigen, Biosens. Bioelectron. 87 (2017) 466–472.
[23] D.B. Liu, X.L. Huang, Z.T. Wang, A. Jin, X.L. Sun, L. Zhu, F. Wang, Y. Ma, G. Niu, A.R. Hight Walker, X.Y. Chen, Gold nanoparticle-based activatable probe for

sensing ultralow levels of prostate-specific antigen, ACS Nano 7 (2013) 5568–5576.
[24] B.Y. Wu, X.P. Yan, Bioconjugated persistent luminescence nanoparticles for Föster resonance energy transfer immunoassay of prostate specific antigen in serum and cell extracts without in situ excitation, Chem. Commun. 51 (2015) 3903–3906.
[25] T. Kaya, T. Kaneko, S. Kojima, Y. Nakamura, Y. Ide, K. Ishida, Y. Suda, K. Yamashita, High-sensitivity immunoassay with surface plasmon field-enhanced fluorescence spectroscopy using a plastic sensor chip: application to quantitative analysis of total prostate-specific antigen and GalNAcβ1–4GlcNAc-linked prostate-specific antigen for prostate cancer diagnosis, Anal. Chem. 87 (2015) 1797–1803.
[26] H.L. Qi, X.Y. Qiu, D.P. Xie, C. Ling, Q. Gao, C.X. Zhang, Ultrasensitive electrogenerated chemiluminescence peptide-Based method for the determination of cardiac troponin I incorporating amplification of signal reagent-encapsulated liposomes, Anal. Chem. 85 (2013) 3886–3894.
[27] Q. Zhao, J. Gao, Sensitive and selective detection of thrombin by using a cyclic peptide as affinity ligand, Biosens. Bioelectron. 63 (2015) 21–25.
[28] S.R. Denmeade, W. Lou, J. Lövgren, J. Malm, H. Lilja, J.T. Isaacs, Specific and efficient peptide substrates for assaying the proteolytic activity of prostate-specific antigen, Cancer Res. 57 (1997) 4924–4930.
[29] H. Qi, C. Wang, X. Qiu, Q. Gao, C. Zhang, Reagent-less electrogenerated chemiluminescence peptide-based biosensor for the determination of prostate-specific antigen, Talanta 100 (2012) 162–167.
[30] D. Wang, Y.N. Zheng, Y.Q. Chai, Y.L. Yuan, R. Yuan, Target protein induced cleavage of a specific peptide for prostate-specific antigen detection with positively charged gold nanoparticles as signal enhancer, Chem. Commun. 51 (2015) 10521–10523.
[31] J. Choi, H. Kim, J. Choi, J. Hong, Y. Kim, B. Oh, A novel Au-nanoparticle biosensor for the rapid and simple detection of PSA using a sequence-specific peptide cleavage reaction, Biosens. Bioelectron. 49 (2013) 415–419.
[32] S.P. Song, Z.Q. Liang, J. Zhang, L.H. Wang, G.X. Li, C.H. Fan, Gold-nanoparticle-based multicolor nanobeacons for sequence-specific DNA analysis, Angew. Chem. Int. Ed. 48 (2009) 8826–8830.
[33] Y. Huo, Liang Qi, X.J. Lv, T. Lai, J. Zhang, Z.Q. Zhang, A sensitive aptasensor for colorimetric detection of adenosine triphosphate based on the protective effect of ATP-aptamer complexes on unmodified gold nanoparticles, Biosens. Bioelectron. 78 (2016) 315–320.
[34] G. Lu, S.Z. Li, Z. Guo, O.K. Farha, B.G. Hauser, X.Y. Qi, Y. Wang, X. Wang, S.Y. Han, X.G. Liu, J.S. DuChene, H. Zhang, Q.C. Zhang, X.D. Chen, J. Ma, Say Chye Joachim Loo, W.D. Wei, Y.H. Yang, J.T. Hupp, F.W. Huo, , Imparting functionality to a metal–organic framework material by controlled nanoparticle encapsulation, Nat. Chem. 4 (2012) 310–316.
[35] X.Q. Cheng, M. Liu, A.F. Zhang, S. Hu, C.S. Song, G.L. Zhang, X.W. Guo, Size-controlled silver nanoparticles stabilized on thiol-functionalized MIL-53(Al) frameworks, Nanoscale 7 (2015) 9738–9745.
[36] S. Su, X.P. Wei, Y.L. Zhong, Y.Y. Guo, Y.Y. Su, Q. Huang, S.T. Lee, C.H. Fan, Y. He, Silicon nanowire-based molecular beacons for high-sensitivity and sequence-specific DNA multiplexed analysis, ACS Nano 6 (2012) 2582–2590.
[37] K.Y. Niu, M. Liu, K.A. Persson, Y. Han, H.M. Zheng, Strain-mediated interfacial dynamics during Au–PbS core–shell nanostructure formation, ACS Nano 10 (2016) 6235–6240.
[38] T.J.A. Slater, A. Macedo, S.L.M. Schroeder, M.G. Burke, P.O. Brien, P.H.C. Camargo, S.J. Haigh, Correlating catalytic activity of Ag–Au nanoparticles with 3D compositional variations, Nano Lett. 14 (2014) 1921–1926.
[39] W.Y. Yu, G.M. Mullen, D.W. Flaherty, C.B. Mullins, Selective hydrogen production from formic acid decomposition on Pd–Au bimetallic surfaces, J. Am. Chem. Soc. 136 (2014) 11070–11078.
[40] D.L. Shao, H.T. Sun, M.P. Yu, J. Lian, S. Sawyer, Enhanced ultraviolet emission from poly(vinyl alcohol) ZnO nanoparticles using a SiO_2–Au core/shell structure, Nano Lett. 12 (2012) 5840–5844.
[41] A.M. Asadirad, N.R. Branda, Two colors of light are needed to break bonds and release small molecules from the surface of SiO_2–Au core–shell nanoparticles, J. Am. Chem. Soc. 137 (2015) 2824–2827.
[42] W.P. Li, P.Y. Liao, C.H. Su, C.S. Yeh, Formation of oligonucleotide-gated silica shell-coated Fe_3O_4-Au core–shell nanotrisoctahedra for magnetically targeted and near-infrared light-responsive theranostic platform, J. Am. Chem. Soc. 136 (2014) 10062–10075.
[43] M. Felber, R. Alberto, ^{99m}Tc radiolabelling of Fe_3O_4–Au core–shell and Au–Fe_3O_4 dumbbell-like nanoparticles, Nanoscale 7 (2015) 6653–6660.
[44] H.L. Ding, Y.X. Zhang, S. Wang, J.M. Xu, S.C. Xu, G.H. Li, Fe_3O_4@SiO_2 core/shell nanoparticles: the silica coating regulations with a single core for different core sizes and shell thicknesses, Chem. Mater. 24 (2012) 4572–4580.
[45] Z.Q. Chu, C. Yin, S.L. Zhang, G. Lin, Q. Li, Surface plasmon enhanced drug efficacy using core–shell Au@SiO_2 nanoparticle carrier, Nanoscale 5 (2013) 3406–3411.
[46] L.K. Ono, F. Behafarid, Beatriz Roldan Cuenya, Nano-gold diggers: au-assisted SiO_2-decomposition and desorption in supported nanocatalysts, ACS Nano 7 (2013) 10327–10334.
[47] J.S. Beveridge, M.R. Buck, J.F. Bondi, R. Misra, P. Schiffer, R.E. Schaak, Mary Elizabeth Williams., Purification and magnetic interrogation of hybrid Au-Fe_3O_4 and FePt-Fe_3O_4 nanoparticles, Angew. Chem. 123 (2011) 10049–10053.
[48] W.L. Hui, F. Shi, K.P. Yan, M.L. Peng, X. Cheng, Y.L. Luo, X.M. Chen, V.A.L. Roy, Y.L. Cui, Z.K. Wang, Fe_3O_4/Au/Fe_3O_4 nanoflowers exhibiting tunable saturation magnetization and enhanced bioconjugation, Nanoscale 4 (2012) 747–751.
[49] V. Urbanova, M. Magro, A. Gedanken, D. Baratella, F. Vianello, R. Zboril, Nanocrystalline iron oxides, composites, and related materials as a platform for electrochemical, magnetic, and chemical biosensors, Chem. Mater. 26 (2014) 6653–6673.
[50] J. Park, K. An, Y. Hwang, J. Park, H. Noh, J. Kim, J. Park, N. Hwang, T. Hyeon, Ultra-large-scale syntheses of monodisperse nanocrystals, Nat. Mater. 3 (2004) 891–895.
[51] Y. Liu, D.L. Purich, C. Wu, Y. Wu, T. Chen, C. Cui, L. Zhang, S. Cansiz, W. Hou, Y. Wang, S. Yang, W. Tan, Ionic functionalization of hydrophobic colloidal nanoparticles to form ionic nanoparticles with enzymelike properties, J. Am. Chem. Soc. 137 (2015) 14952–14958.
[52] S. Lee, J. Noh, S. Hong, Y.K. Kim, J. Jang, Dual stimuli-responsive smart fluid of graphene oxide-coated iron oxide/silica core/shell nanoparticles, Chem. Mater. 28 (2016) 2624–2633.
[53] M. Li, X. Li, X. Qi, F. Luo, G. He, Shape-controlled synthesis of magnetic iron oxide@SiO_2–Au@C particles with core–shell nanostructures, Langmuir 31 (2015) 5190–5197.
[54] D.J. Maxwell, J.R. Taylor, S.M. Nie, Self-assembled nanoparticle probes for recognition and detection of biomolecules, J. Am. Chem. Soc. 124 (2002) 9606–9612.